Lasers in Manufacturing Conference 2025

Determining the Electrical Properties and Proportionality Factor of Digitally Printed and Laser-sintered Strain Gauges for Tensile Strain Measurements

Martin Shulevski[a,*], Siwar Darawshe[b], Adam El-Sarout[a], Samuel Fink[a]

[a]*Fraunhofer Institute for Laser Technology, Steinbachstraße 15, 52074 Aachen, Germany*
[b]*RWTH Aachen University, Campus Boulevard 53, 52074 Aachen, Germany*

Abstract

Integrated sensors are becoming increasingly important for structural health monitoring (SHM) of components. Additively manufactured strain gauges can be used to evaluate the mechanical stress of materials with sensitivity comparable to that of manually applied strain gauges. We propose an approach that involves the application of strain gauges to metal components using an inkjet printing process with a nanoparticle silver ink. In a post-processing step, the strain gauges are laser-sintered to functionalize the material and adjust the resistivity of the thin film. The strain gauges presented exhibit resistance values from 320 Ω to 520 Ω. We report on the results of tensile tests with the contacted sensors and characterizing their electrical properties, as well as the proportionality factor of the strain gauges in dependence of the laser process parameters. The electromechanical characterization of the 200 nm thick strain gauges for different sintering parameters yields strain gauge factors ranging from 0.35–0.68, which remain stable throughout strain measurements. With a hysteresis error smaller than 1% and an electrical drift not surpassing 10%, the strain gauges show high sensitivity, reliability and flexibility.

Keywords: printed electronics; strain gauges; inkjet printing; laser-sintering; tensile strain measurement; sensor integration; structural health monitoring.

1. Introduction

Structural health monitoring (SHM) of materials and components is becoming increasingly important in safety-critical areas such as automotive, mechanical and production engineering, aviation and construction. The aim of structural health monitoring is the detection of deformations, cracks or material fatigue at an early stage to safeguard operational safety, reduce maintenance costs, and extend the service life.

Resistive strain gauges (SG) which convert mechanical strain into electrical signals have become increasingly important for SHM systems. Conventional strain gauges require complex lithographic production or spin-coating (Maiwald, 2010) which are associated with high material consumption, multiple fabrication steps, high processing temperatures, and limited design freedom (Kale, 2012). The advantages of conventional strain gauges are the reliable properties and a low signal-to-noise (SNR) ratio. However, the manual application of conventional strain gauges can lead to variations in the sensor performance.

In contrast, additively manufactured strain gauges produced by using direct printing techniques such as inkjet printing have received growing attention for the application of sensors. Inkjet printing is a digital, non-contact method with precise control of the quantity of applied ink and layer thickness (Correia, 2013). This enables almost complete flexibility in the design of the printed strain sensors, as they can be applied directly onto complex surfaces, albeit with significant limitations, as well as flexible surfaces. Therefore, they are ideal for integrated sensor systems and for saving costs and materials.

In this study, we investigate the effects of the laser power P_L and the scan speed v_S on the laser sintering process of our printed structures. This way, the influence of the laser parameters on the precise adjustment of the sensor conductivity is quantified, offering a stable, energy-efficient and reproducible method for functionalization of our thin layers with short processing time and no damage to the underlying substrate.

2. Experimental details

The strain gauge sensors are manufactured with a commercially available water-based nanoparticle silver ink for the inkjet printing process. They are then functionalized with a laser sintering process in which the silver nanoparticles are fused together to form continuous, conductive structures.

Quarter-bridge strain gauge structures have been printed on flat probes for tensile strain measurements and laser-sintered with varying laser power P_L and the scan speed v_S with the goal of achieving specific resistance values. The sensors were contacted with wires and conductive silver paste on their contact pads (fig. 1 (a)). The samples were positioned in a tensile strain testing machine and the resistance change of the resistive sensors with applied tensile strain was recorded. After data analysis the proportionality factor (also strain gauge factor) of our sensors, their hysteresis behavior as well as their electrical drift were determined and evaluated.

2.1. Application of isolation layer

As mentioned in the previous section, additive manufacturing processes offer the advantages of contactless, flexible and precise application of different materials on various substrates. For our experiments we use planar stainless steel tensile strain samples with dimensions 180 mm × 15 mm × 0.9 mm for sensor application. For the printing of the strain gauges, it is necessary to deposit an isolation layer on the steel tensile strain samples before applying the strain gauge.

A commercially available thermosetting polymer named OrmoComp® from the manufacturer Micro Resist Technology, which is liquid at room temperature with a viscosity of 500 mPa·s, is loaded into the cartridge of a Martin Clever Dispense 06 Pro dispenser. The isolation layer is applied onto the tensile strain probes with a needle dispenser with a needle diameter of 0.34 µm. The volume flow rate through the needle is 7 mm^3/s with a speed of 12 mm/s. The motion of the 3-axes-dispense-system is controlled by a G-Code script following a helical path to create square layers with the size of 27 mm × 12 mm in the middle of the tensile strain samples. After dispensing, the isolation layers are hardened used a UV lamp with a wavelength of 365 nm for 20 min.

The profile measurements with the Keyence Dektak profilometer show an average layer thickness of 102 ± 6 µm across all dispensed samples with a smooth and even surface starting 3 µm away from the layer edges.

Subsequently, the samples are placed in an argon plasma chamber at a pressure of 0.4 mbar for surface treatment of the isolation polymer surface. The aim is to increase the surface energy and improve the wettability and adhesion of the metal ink.

2.2. Inkjet printer of conductive silver ink

Inkjet printing of the strain gauges is carried out with a Fujifilm Dimatix DMP-2850 Material Printer with Samba Materials Cartridge with a maximum fluid volume capacity of 1.5 ml. The 12 cartridge printing nozzles have a diameter of 30 µm and a native drop volume per nozzle of 2.4 pl.

The Dimatix DMP-2850 printer allows the user to define a large set of parameters such as the cartridge temperature, substrate platen temperature, nozzle voltage and nozzle frequency so that printing can be optimized depending on the substrate, ink (important here are the viscosity and surface tension) and application.

A commercially available aqueous and nanoparticle silver ink AS-J102 from Novacentrix is used for printing. A double waveform was used for the electrical voltage signal for the nozzles with a corresponding frequency of 5 kHz and a total deposition wave time of 12.1 µs per volume droplet. The nozzle voltages ranged from 20 V to 25 V and were adjusted in such a way that all volume droplets were uniformly jetted. After printing, the ink is dried on the platen substrate holder at a temperature of 45 °C.

2.3. Laser sintering of printed structures

An Ytterbium fiber laser from IPG Photonics with a wavelength of 1064 nm and a maximum output power of 200 W is used for laser sintering the printed structures. The beam has a top-hat profile and is focused via a F-Theta scan lens from THORLABS with a focal length of 254 nm which result in a spot diameter of 800 µm.

As previously mentioned, the laser power P_L and the scan speed v_S are varied, while the hatch distance Δy is kept constant at 40 µm. This was done with the goal of sintering the printed sensors while varying these two parameters in a 2D matrix (fig. 1 (b)) and measuring the resistance values of the printed strain gauges for each parameter set. The average intensity I_A of the laser is calculated and used to specify the process conditions:

$$IA = \frac{P_L}{A} = \frac{P_L}{\pi r^2} \quad (1)$$

Eq. (1) describes the ratio between the laser power P_L and the spot surface area.

After sintering, the conductive tracks of the SG are encapsulated by dispensing an isolation layer, while leaving the contact pads uncovered for contacting, and hardened as previously explained. This way, the printed SG are protected from external mechanical damage.

2.4. Electrical resistance measurement

The direct current electrical resistance of the single sensors after sintering and contacting is measured at room temperature with a Keysight U1272A True RMS digital multimeter with a precision of measurement of 0.05% in DC mode. The contact cables of the multimeter are connected to the two contact pads of each strain gauge and the resistance is measured; the multimeter connector clamps have a contact resistance of 0.3Ω. This measurement allowed the characterization of the sensor before deformation; the measured resistance values are indicated as R_0 for each strain gauge.

2.5. Electro-mechanical characterization of the printed strain gauges

The strain gauge factor (GF or proportionality factor) is a fundamental parameter of a printed strain gauge sensor characterizing its sensitivity to deformation. The strain gauge factor can be characterized as the ratio between the relative change of the electrical resistance and the relative mechanical deformation:

$$GF = \frac{\left(\frac{\Delta R}{R_0}\right)}{\left(\frac{\Delta l}{l_0}\right)} = \frac{\left(\frac{\Delta R}{R_0}\right)}{\varepsilon} \quad (2)$$

In eq. (2), the value R_0 corresponds to the resistance value without deformation of the sample. ΔR is the relative electrical resistance change of the strain gauge caused by the deformation due to tensile strain given by the variation of the length Δl relative to the initial length of the sample l_0 (Correia, 2013), the latter two of which can be expressed by the mechanical strain ε.

The electromechanical characterization is achieved with repeated singular uniaxial and cyclical uniaxial tensile strain measurements at room temperature for determining the GF. During the tensile strain measurements, the electrical resistance change is recorded. From the mechanical data (the strain values) as well as the electrical data (resistance change values) a curve for each displacement is plotted. The SG proportionality factor is determined by linear regression. For cyclical uniaxial measurements, the value of the SG factor is determined for each loading/unloading cycle to examine the replicability of the results or the change of the SG factor over the course of repeated straining. This can be evaluated by determining the hysteresis error γ:

$$\gamma = \left|\frac{\Delta R_{load} - \Delta R_{unload}}{\Delta R_{max}}\right| \cdot 100\% \quad (3)$$

In eq. 3, (ΔR_{load} - ΔR_{unload}) is the maximum difference in resistance at the same strain for the loading and unloading curves in a cycle of a cyclical measurement, while ΔR_{max} represents the maximum change in resistance over the entire strain gauge measurement. A hysteresis loop and the parameters necessary for determining γ are shown in fig. 1 (c).

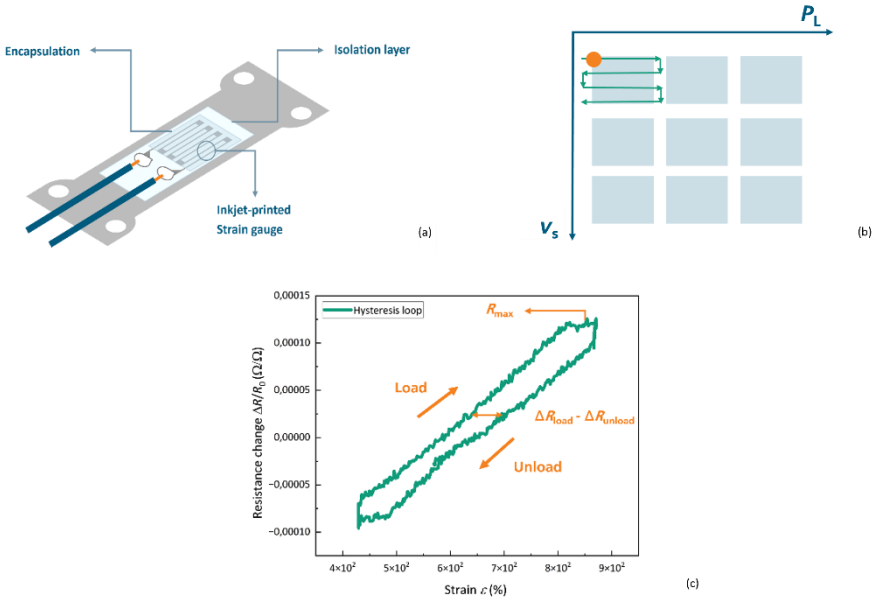

Fig. 1. (a) Schematic diagram of the processing steps for the sample preparation; (b) 2D matrix for determining the laser sintering parameters of square printed structures as well as the applied scanning strategy; (c) Examining a single hysteresis loop for determining the hysteresis error in a cycle load for a laser-sintered strain gauge strain gauge.

3. Result and discussion

3.1. Development of strain gauges

The pattern for the quarter-bridge strain gauge sensors is shown in fig. 2 (a). With a surface of 22.5 mm × 10 mm, the strain gauge is designed for a drop spacing of 25 µm, which equals an image resolution of 1016 dpi (dots per inch). Microscopic images in fig. 2 (b) show inkjet-printed structures with conductive tracks that are 170 µm wide.

The most homogenous printing results are achieved when the movement of the printhead is parallel to the conducting paths in the sensors (Correia, 2013). For this reason, the quarter-bridge strain gauges were printed along the longitudinal direction (long axis) of the tensile strain gauges.

To investigate suitable functionalization parameters for the laser sintering of strain gauges, test structures in the form of rectangles with 6 mm × 5 mm are printed onto isolation layers dispensed on microscope glass slides. These structures were arranged in a 5 × 3 test matrix.

3.2. Laser functionalization

For laser sintering of the test matrices with square fields, the scanning speed and the laser power are specifically varied to investigate the conductivity of the printed structures, while the hatch distance was kept constant at 40 µm.

Two curves for scan speeds of 1000 mm/s as well as 1750 mm/s for varying laser power shows the tendencies for high and stable conductivity for P_L between 30 W and 35 W (or I_A between 14.9 W/mm² and 17.4 W/mm²), as shown in fig. 2 (c).

The resistance values from both curves show large standard deviations for 5 samples processed with the same conditions for P_L < 30 W. This could arise from incomplete sintering; the thermal energy in the intensity range from 9 W/mm² to 14 W/mm² is insufficient for continuous and even-distributed sinter neck formation in the metallic nanoparticle network. Cross-linking of nanoparticles improves with rising intensity, leading to lower resistance values. Both curves show an optimum range with a local maximum for the resistance values around P_L of 32 W. The curve for v_S of 1000 mm/s during sintering exhibits a stable sintering process for laser power above 32 W with a standard deviation of around 10%, suggesting a more uniform energy delivery and nanoparticle fusion. The curve for v_S of 1750 mm/s shows a rising flank for higher laser power for P_L > 32 W, indicating an introduction of defects in the percolation network (Rehberger, 2022).

In addition to achieving the lowest possible resistance values during sintering (tab. 1), a stable range with minimal deviations from the achievable resistance values is important to ensure a reliable and reproducible process.

Table 1. Laser sintering parameters for the samples prepared for the presented experiments' results.

Scan speed v_S (mm/s)	Laser power P_L (W)	Resistance R_0 (Ω)
1000	22	511
	32	320
1750	32	474
	40	387

3.3. Electromechanical measurements and characterization of electrical properties of strain gauges

In order to determine the sensitivity to deformation of the inkjet-printed and laser functionalized strain gauges, a ZwickRoell tensile testing machine is used to apply mechanical strain to the tensile samples. The tensile tests are performed using ZwickRoell's testXpert III software, which controls the testing machine and enables continuous recording of force, strain and measurement time. The sensors are contacted with conductive silver glue on their contact pads with cables and connected to a QuantumX MX840B amplifier from HBK, while the data was recorded and analyzed using the Catman Easy data analysis software on an external laboratory PC. As soon as tensile strain is applied during the measurement, the change in resistance triggers the recording of the resistance change curve of the SG.

The singular uniaxial tensile strain measurements are strain controlled and carried out with a maximum strain force F_S of 350 N, a limitation set by the elasticity of the tensile samples, and tensile strain rates $\dot{\varepsilon}$ of 0.001%/s and 0.0001%/s. The results of the measurements are depicted in fig. 3 (a) and fig. 3 (b). The results show a linear response of the strain gauges to the applied deformation in longitudinal direction caused by tensile strain. At the higher rate $\dot{\varepsilon}$ of 0.001%/s, the resistance change of the SG follows the force strain curve F_S precisely. At the lower rate of 0.0001 %/s, the rise of resistance change appears straighter, but also exhibits more noise. The latter could be explained by low Signal-to-Noise Ratio (SNR) due to the small signal amplitude per time unit, making noise more prominent during the measurement. The microstructural rearrangement of the nanoparticle mesh grid could be coupled with 1/*f*-noise (or flicker noise), which is more dominant in low-frequency measurements.

The strain gauges are functionalized with different laser sintering parameters, meaning that their resting resistance values R_0 differ before mechanical deformation. The singular uniaxial strain tests show that varying laser sintering parameters influence different initial proportionality or gauge factors. For example, strain gauges laser-sintered with P_L of 32 W, v_S of 1750 mm/s and subjected to uniaxial strain tests result in slightly different GF: for $\dot{\varepsilon}$ of 0.0001%/s the GF is 0.48 ± 0.00023, while for $\dot{\varepsilon}$ of 0.001%/s the GS is 0.4512 ± 0.0016.

Repetition of single uniaxial measurements, meaning conducting the same test after relaxation, shows a slight change in the GF of the strain gauges, which could be the result of microstructural changes and the introduction of cracks and defects, and the building of new percolation networks affecting the conductivity of the functionalized silver sensors. (Cochrane, 2010)

Cyclical uniaxial tensile strain measurements with 10 load cycles, a maximum strain force F_S of 300 N as well as a strain force rate $\dot{\varepsilon}$ of 0.001 %/s were carried out to test the repeatability and electrical drift of the sensor signals. Again, strain gauges functionalized with P_L of 32 W and v_S of 1750 mm/s were subjected to cyclic loading.

The sensor signal response follows the flanks of each cycle, but a general increase of the resistance change is noticeable with each following cycle, since the idle period of 3 s between cycles is insufficient for the mesh grid relaxation (depicted in fig. 4 (a)). The mean GF for the first cycle load is 0.46 ± 0.00023 with a hysteresis error γ of 0.36%. The GF for the tenth and last cycle load is 0.68 ± 0.04, indicating an increase in GF throughout the measurement period, alongside an increase in electrical drift denoted by a γ of 0.89% (as can be seen in fig. 4 (b)). This is suggestive of an incipient deviation or structural change within the SG structure, which may be caused by plastic deformation of the tensile strain probes and the isolation layer, even if the strain was kept within the elastic strain region of the tensile strain probes (Cochrane, 2010). Another possible explanation could be given by the reorganizing of the nanoparticle network during the cycle loads. Any disconnections created during elongation are then, in theory, re-connected during contraction. However, if the disconnections between nanoparticles in the mesh grid are not re-connected, the overall electromechanical properties of the sensor are modified with each cycle load (Cochrane, 2010).

The hysteresis error values remain low and stable throughout the conducted measurements. A stable strain gauge has a hysteresis error of less than 5%. Values above this limit indicate a delayed or non-linear return of the electrical signal during unloading, which can lead to measurement errors under cyclical loading conditions. The contrary was true in this case, confirming the stability of the functionalized strain gauges under different mechanical strain conditions.

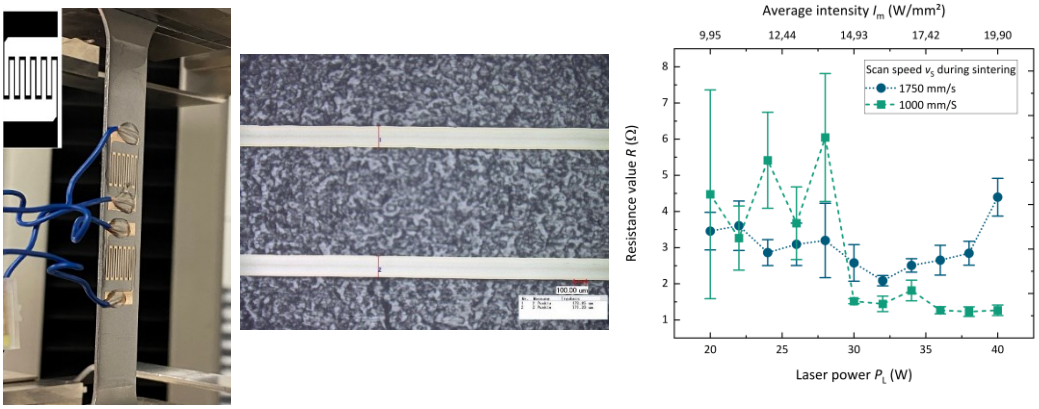

Fig. 2. (a) Contacted and functionalized inkjet-printed strain gauges with a depiction of the digital sensor design; (b) Microscopic image of the conductive tracks of the strain gauges and determining their width of 170 µm; (c) Curves for dependance of resistance values from the laser sintering power.

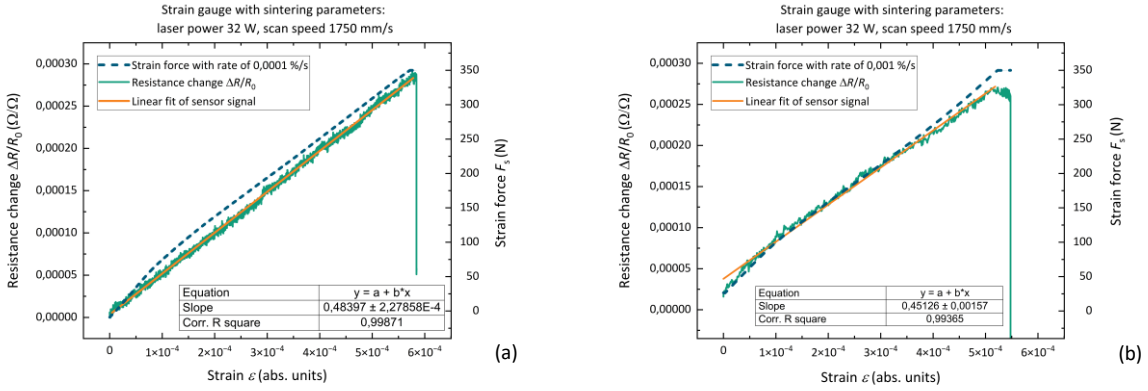

Fig. 3. Single uniaxial strain measurement of strain gauges sintered with P_L of 32 W and v_S of 1000 mm/s with the tensile strain force condition parameter of 350 N and a strain rate of (a) 0.0001 %/s; (b) 0.001 %/s.

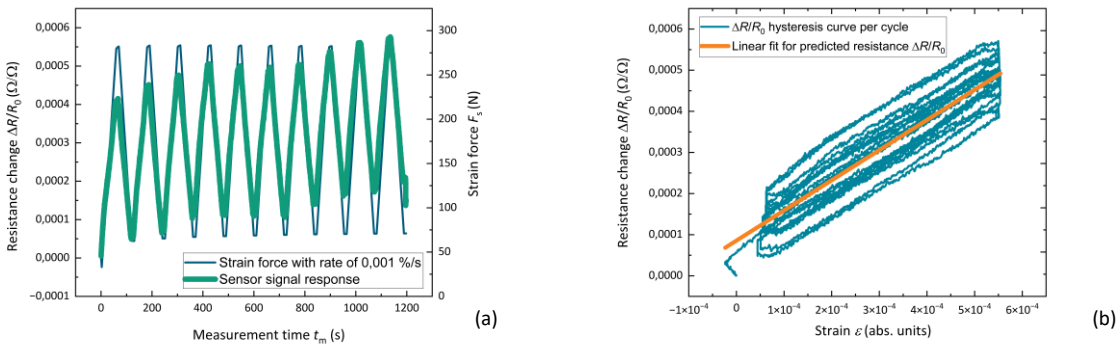

Fig. 4. (a) Cyclic uniaxial strain measurement of a strain gauge sintered with P_L of 32 W and v_S of 1000 mm/s with the tensile strain force condition parameter of 300 N and a strain rate of 0.001 %/s; (b) Relative change in the electrical resistance due to continuous mechanical deformation for 10 cycle loads.

4. Conclusions

Multiple quarter-bridge strain gauges (SG) with the same architecture are inkjet-printed with a conductive nanoparticle silver ink on flat tensile strain samples covered with a polymer isolation layer. Sensors with dimensions of 22.5 mm × 10 mm were laser-sintered with scan speed v_S of 1750 mm/s and laser power P_L of both 32 W and 40 W to functionalize the thin film layers and adjust the resistance values, which were 474 Ω and 387 Ω, respectively.

The electromechanical characterization of the sensors is conducted in a tensile testing machine in two sets of experiments: singular uniaxial and cyclical uniaxial loading. Initial singular uniaxial measurements show a linear response in the change of electrical resistance to the linear strain, as well as little variation of the gauge factors (GF) in dependance of the laser power and scan speed in the laser functionalization step. However, the strain rate of the tests determined the type of structural stress introduced in the nanoparticle networks, and with it, the strain gauge factor.

Cyclical uniaxial loading again showed a linear response to the strain cycles gauges with little relaxation time in between. This caused a continuous rise in electrical drift of the strain gauge, accompanied by an increase of the GF from 0.46 ± 0.22 to 0.68 ± 0.04. The hysteresis error γ of the individual load-unload hysteresis curves increases parallel to the drift from 0.36% to 0.89%, as expected. However, γ does not surpass the 5% mark for the maximum achievable hysteresis error, confirming the assumption that the laser functionalization of inkjet-printed strain gauges leads to high sensitivity, reliability and flexibility.

Further experiments are necessary to investigate the crack formation due to physical deformation in the SG and model its influence on the change of conductivity and GF under the influence of varying strain rate $\dot{\varepsilon}$ and straining cycles This could help better understand the behavior of the laser-sintered sensors and lead to a proof-of-principle in practical applications.

References

Maiwald, M. W. (2010). INKtelligent printed strain gauges. *Sensors and Actuators A: Physical vol 162*, 198-201.

B., K. B. (2012). Ink-jet printed conducting polyaniline based flexible humidity sensor. *IMSC 2012: 14 Int. Mtg on Chemical Sensors*, 1112-5.

Correia, V. C.-M. (2013). Development of inkjet printed strain sensors. *Smart Materials and Structures 22. IOP Publishing*.

Kale, B. B. (2012). Ink-jet printed conducting polyaniline based flexible humidity sensor. *IMCS 2012: 14th Int.Mtg on Chemical Sensors,*, 1112-5.

Rehberger, M. M. (2022). Rotation Grids for Improved Electrical Properties of Inkjet-Printed Strain Gauges. *Sensors 2022, vol. 22*, 6113.

Cochrane, C. L. (2010). A Flexible Strain Sensor Nased on a Conductive Polymer Composite for in situ Measurement of Parachute Canopy Deformation. *Sensors*, 8291-8303.